Tellus (1988), *40B*, 23–41

Dry deposition velocities of atmospheric aerosols as inferred by applying a particle dry deposition parameterization to a general circulation model

By FILIPPO GIORGI, *National Center for Atmospheric Research*, P.O. Box 3000, Boulder, Colorado 80307, USA*

(Manuscript received October 29, 1986; in final form February 4, 1987)

ABSTRACT

A particle dry deposition parameterization is applied to a general circulation model to carry out a diagnostic study of global scale dry deposition velocities of ambient aerosols. Bulk deposition velocities are calculated for observed nuclei, accumulation, and coarse modes using two models, one with a more complete description of surface processes. Seasonal as well as diurnal effects are analyzed. The spatial and temporal variability of deposition velocities depends in a complex fashion on both microphysical (particle size and characteristics of the surface elements) and meteorological (surface wind speed and atmospheric stability near the surface) variables. For individual snapshots, mass-average dry deposition velocities are found to lie in the range of 0.01–0.2 cm/s for the nuclei mode, 0.001–0.05 cm/s for the accumulation mode, and 1.25–5 cm/s for the coarse mode. When averaged over long-term simulations, the corresponding values are 0.015–0.15 cm/s, 0.002–0.03 cm/s, and 1.25–3.5 cm/s, respectively. Averaged deposition velocities are larger over vegetated areas than over snow, bare ground, and ocean surfaces by a factor of about 1.5–3 and seem also to be sensitive to different vegetation types. Over oceans, the deposition rates tend to mainly correlate with the surface wind speed patterns. Over land areas, however, the effect of the surface thermal response to insolation on convective mixing in the boundary layer becomes important, especially in conditions of small mean solar zenith angle. In this case, the deposition velocity shows a marked diurnal trend, being larger during daytime than during nighttime by a factor of 1.5–2.5. The seasonal variation of surface wind speed and insolation, thus, affects the deposition patterns. Diffusiophoresis related to water evaporation over ocean surfaces is shown to possibly play an important rôle in inhibiting deposition of accumulation-mode particles.

1. Introduction

Dry deposition of atmospheric aerosols (i.e., deposition on the earth's surface not related to precipitation) is a very complex process that depends upon meteorological conditions near the surface, particle properties, and characteristics of the surface roughness elements. Because of these dependencies, particle deposition can be highly variable in space and time. This variability in turn affects the deposition patterns of aerosols that may have significant environmental and/or climatic impacts. As illustrations, acid deposition in Europe and in regions of United States and Canada, the phenomenon of Arctic Haze, and the "nuclear winter" hypothesis are related to possible effects of perturbations of the atmospheric particulate loading. Since dry deposition is one of the processes that regulate the atmospheric residence time of aerosols, it is important to determine the sensitivity of the corresponding deposition rates to relevant physical factors.

In a previous paper (Giorgi, 1986; hereafter referred to as GI), following a semiempirical approach, the author developed a particle dry

* The National Center for Atmospheric Research is sponsored by the USA National Science Foundation.

deposition parameterization scheme that explicitly describes the effects of meteorological variables and particle dynamics on the dry deposition velocity, the ratio of particle flux to particle concentration at a specified reference height. The scheme is designed to be incorporated into tracer-transport models by acquiring from the "host model" a number of surface meteorological variables and surface characteristics. In the present work, the GI parameterization is applied to a general circulation model (GCM) to calculate dry deposition velocities of atmospheric aerosols. The purpose here is to investigate on a global scale, using a realistic description of atmospheric circulation generated by an operational GCM, the spatial and temporal variability of calculated deposition velocities as affected by meteorological and microphysical variables. As we will see, the flexibility of the GI parameterization scheme renders it particularly suitable for such a study.

Although the extension of semiempirical descriptions of dry deposition to field conditions is rather tentative and may be subject to large uncertainties, a diagnostic study of this type can be useful both for deposition assessment and modeling purposes. First, it provides first-order estimates of deposition rates for observed aerosol distributions under a number of simulated, but realistic, atmospheric conditions. Second, it emphasizes the relative importance of, and the possible interactions among, the different physical factors that affect the deposition process, and as a consequence, the importance of including such dependencies in simulations of atmospheric particulate budgets. The interest of carrying out such an analysis on a global scale is then raised by the increasing concern about possible global climatic and environmental effects of atmospheric injections of particulate material (of natural and/or anthropogenic origin).

In the following sections, first the basic characteristics of the GI dry deposition parameterization scheme will be briefly reviewed. Mass-average deposition velocities will then be calculated on a global scale for different observed aerosol distributions, on several types of surfaces, as a function of time and space. To determine the influence on the simulated particle dry deposition velocities of an accurate treatment of surface processes, results will be presented as obtained using two models, one with a more accurate description of the atmospheric boundary layer. Diurnal as well as seasonal effects will be analyzed.

2. A parameterization scheme for particle dry deposition on different types of surfaces

In this section, we will briefly review the particle dry deposition parameterization scheme of GI (for details the reader is referred to the original paper). This scheme makes use of a two-layer boundary layer model consisting of an "interfacial layer" of depth δ (depending on the type of surface), immediately adjacent to the earth's surface, and a "surface layer" extending from the height δ to the height h of the bottom level of the host transport model. Steady state conditions are assumed, that is, the particle flux is assumed to be constant throughout the layer extending from the surface to the level h (note, however, that this assumption becomes less accurate as h increases). Transfer of aerosols through the surface layer is dominated by gravitational settling and by turbulence, for which it is assumed that particle transfer occurs at the same rate as momentum transfer. This approximation has been widely used for modeling purposes (e.g., Slinn, 1982; Slinn and Slinn, 1980), and was preferred in the development of this particle deposition parameterization for two reasons. First, most of the available laboratory studies used to derive the expressions for the particle deposition velocity reported only quantities, such as the friction velocity, describing momentum flux to surfaces. Second, many dynamical models, in particular current operational GCMs, make use of the surface drag coefficient to parameterize momentum as well as heat and water vapor transfer to the surface. As also pointed out by one of the reviewers, however, an analogy to heat transfer through the surface layer would probably be more correct and should in the future be investigated. Transfer through the interfacial layer includes the contributions of Brownian diffusion, interception, and impaction on the surface roughness elements, diffusiophoresis over evaporating or condensing water surfaces, and again, gravitational settling. Electrical and thermophoretic effects are neglected.

The scheme produces particle deposition velocities relative to the height h expressed in terms of wind speed, temperature, and air density at the bottom level of the host transport model, surface momentum drag coefficient (usually provided by the host model), particle size and density, characteristics of the surface roughness elements and several parameters derived for different surface types. Four surface types are considered: smooth surfaces (such as snow and water surfaces at low wind speeds), surfaces with bluff roughness elements (bare soil fields, developing water waves, irregular ice and snow surfaces, and many urban environments), ocean surfaces, and vegetative canopies.

Table 1 shows the expressions obtained in GI for the surface deposition velocity, and related model quantities, over the various surface types (details on the derivation of these relations can be found in GI). Figs. 1 and 2 show examples of particle deposition velocities over oceans and vegetative canopies as predicted by (a)–(h) of Table 1 (these figures and other aspects of this parameterization scheme are discussed in detail in GI). In general, deposition velocities predicted by (a)–(h) are minimum in the size range $r = 0.05$–1 μm, in which they assume values of 0.005–0.1 cm/s for $u_* = 20$–200 cm/s, where r is the particle radius and u_* the friction velocity. They then increase for lower and higher particle sizes (owing to the increasing efficiency of Brownian diffusion and impaction, respectively) and with wind speed and surface drag coefficient (owing to the more effective turbulent transport through the surface layer). These deposition velocities are generally consistent with laboratory measurements of particle deposition over grass and other types of short vegetation (e.g., Chamberlain, 1967; MacMahon and Denison, 1979) and with predictions of semiempirical models based on laboratory data (e.g., Slinn, 1977, 1982). They are also consistent with the field data of Jonas and Heinemann (1985), who measured deposition velocities for radioactively tagged mono- and polydispersed aerosols with radii in the range of 0.2–8.5 μm on water, smooth surfaces, and various types of vegetation. Jonas and Heinemann found, for example, that the deposition velocity over grass, at $u_* = 30$ cm/s, varied from about 0.01 cm/s for $r \simeq 0.5$ μm to about 5 cm/s for $r \geqslant 5$ μm, decreasing by a factor of $\simeq 3$ for water and smooth surfaces, and increasing for various kinds of forests (these last estimates based on model considerations).

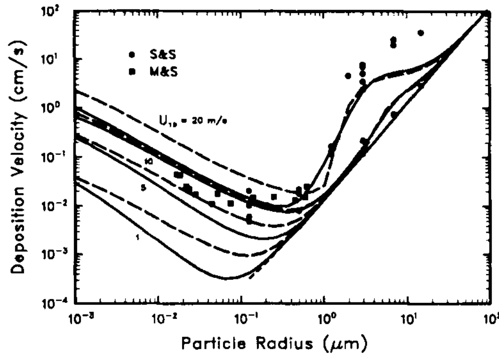

Fig. 1. Deposition velocity on oceanic surfaces at the height $h = 10$ m, as a function of the wind speed at 10 m (U_{10}), for 1 g/cm^3 density particles, as predicted by using (a)–(h) of Table 1 (solid curves) and by the model of Slinn and Slinn (1980) (dashed curves). Also shown are the deposition data of Moller and Schumann (1970) (M&S) and Sehmel and Sutter (1974) (S&S). For the M&S data the wind speed was in the range of 3–8 m/s; for the S&S data the wind speed was in the range of 2–14 m/s.

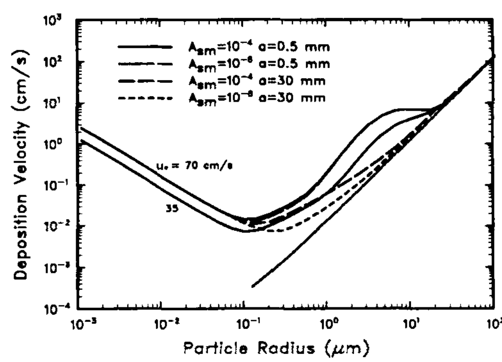

Fig. 2. Dependence of 1 g/cm^3 density particle deposition velocity on friction velocity u_*, "large collector" projected radius a, and "small collector" collection parameter A_{sm} (see Table 1 and GI), as predicted using (a)–(h) of Table 1. Other parameter values used for these calculations are $C_D = 3 \times 10^{-2}$, $C_{D_0}^{-1/2} = 2.5$, $c_v/c_d = 1/3$, $c_d = 0.3$, $a_{sm} = 10$ μm (see Table 1 and GI). These parameter values are typical of grass and other types of vegetative canopies (e.g., Slinn, 1982). Note that particle rebound is also included via the factor f_{BO} of Table 1.

Eddy-correlation measurements of submicron aersols' deposition velocities yield values that are

Table 1. *Reference equations and related parameters for particle dry deposition calculations as inferred from the dry deposition parameterization scheme of Giorgi (1986)*

Reference equation	
$\phi_h = v_{dep} n_h$	(a)
$v_{dep} = K_{dep} + K_{dh}$	(b)
$K_{dep} = \dfrac{K_{SL}(K_{IL} f_{BO} + K_{d\delta} - K_{dh})}{K_{SL} + K_{IL} f_{BO} + K_{d\delta}}$	(c)
$K_{SL} = C_D U_h A_p \dfrac{C_{D_0}^{1/2}}{C_{D_0}^{1/2} - C_D^{1/2}}$	(d)
$K_{IL} = C_{D_0}^{1/2} u_* G$	(e)
$K_{dh} = v_g$	(f)
$K_{d\delta} = v_g + v_{dph} = v_g + 10^3 \dot{m}$	(g)
$G = B_{st} C_{D_0}^{-1/2}$	(h)

Surface type	$C_{D_0}^{-1/2}$	G
Smooth ($Z_{0+} \leqslant 0.13$)	13.5	$Sc^{-2/3} + 4.72 St^2 (St^2 + 400)^{-1}$
Transition (bluff rough. elem.) ($0.13 \leqslant Z_{0+} \leqslant 2$)	$6.432 Z_{0+}^{-0.3634}$	$0.6667 Z_{0+}^{-0.2} Sc^{(-0.538 Z_{0+}^{-0.105})} + 2.25 Z_{0+}^{-0.3634} St^2 (St^2 + 400)^{-1}$
Fully rough (bluff rough. elem.) ($Z_{0+} \geqslant 2$)	5	$0.6849 Z_{0+}^{-0.25} Sc^{-1/2} + 1.75 St^2 (St^2 + 400)^{-1}$
Vegetative canopy	2.5	$(\eta/c_d)^{1/2}$ where, $\eta = c_v Sc^{-1/3} + R^2/2 + St_a^{3.2}(St_a + 0.6)^{-3.2} + A_{sm} R_{sm} \ln(1 + R_{sm})$; $c_d = 0.2$–0.5; $c_v/c_d \simeq 1/4$–$1/3$; $A_{sm} \simeq 10^{-5} - 10^{-4}$; $f_{BO} = e^{-\sqrt{St_a}}$
Ocean	$Z_0 = 0.015 \dfrac{u_*^2}{g}$ then, depending on the value of Z_{0+}, formulas for smooth to fully rough surfaces are used; f_{BO} is set equal to 1	

about an order of magnitude larger than those of Fig. 2 (e.g., Wesely et al., 1985). The limitations of the eddy-correlation technique in measuring small deposition velocities, however, have been pointed out and extensively discussed (Slinn, 1983; Wesely et al., 1985). Moreover, radionuclides deposition observations have been recently used to estimate deposition velocities of small particles on vegetation of the order of 0.03–0.06 cm/s, i.e., closer to model-derived values (Russell et al., 1981; Lindberg et al., 1982; Bondietti et al., 1984). A large uncertainty is thus present in current field estimates of aerosol dry deposition velocities, an uncertainty that probably exists also for the present calculations.

In the next sections the parameterization scheme of GI will be applied to a GCM to calculate global scale dry deposition velocities of aerosols of continental origin. Whitby and Cantrell (1975) and Whitby (1978) have shown that the distribution of most continental aerosols can be approximated by the sum of three modes, the nuclei mode (NM), the accumulation mode (AM), and the coarse mode (CM), each

Table 1 *continued*

List of symbols used in this table	
a	Projected radius of the surface roughness elements
a_{sm}	"Small collector" projected radius
A_p	Ratio of particle diffusivity and momentum eddy diffusivity = 1
A_{sm}	"Small collector" collection factor
B_{st}	Particle surface Stanton number = K_{IL}/u_*
c_d	Average drag coefficient for single surface roughness elements
c_v	Average viscous drag coefficient for single surface roughness elements
C_D	Surface drag coefficient relative to the height h
$C_{D\delta}$	Surface drag coefficient relative to the height δ
D	Particle diffusivity
f_{BO}	Rebound factor
g	Gravity constant
h	Upper edge of the surface layer corresponding to the bottom level of the host transport model
k	Von Karman constant
$K_{d\delta,dh}$	Particle drift velocity at the height δ, h
K_{dep}	Overall particle surface transfer velocity
K_{IL}	Interfacial-layer particle transfer velocity
K_{SL}	Surface-layer particle transfer velocity
$\dot{m}$	Rate of water evaporation (g cm^{-2} s^{-1})
n	Particle concentration, i.e., number of particles of a given size per unit volume, at the height h
r	Particle radius
R	Interception parameter = r/a
R_{sm}	"Small collector" interception parameter = r/a_{sm}
Sc	Schmidt number = ν/D
St	Stokes number = $\tau_{rel} u_*^2/\nu$
St_a	Stokes number = $\tau_{rel} u_*/a$
u_*	Friction velocity
U_h	Wind speed at level h
v_{dep}	Particle deposition velocity (at the height h)
v_{dph}	Diffusiophoretic drift velocity
v_g	Particle gravitational settling velocity
Z_0	Surface roughness height
Z_{0+}	Roughness Reynolds number = $Z_0 u_*/\nu$
δ	Height of the interfacial layer
η	Particle collection efficiency of the single roughness elements
ϕ_h	Particle flux, positive downward, at the height h (assumed to be equal to the flux at the surface)
ν	Air's kinematic viscosity
τ_{rel}	Particle relaxation time = v_g/g

characterized by a log-normal size distribution of the form

$$\frac{dn}{dr}dr = \frac{N}{\sqrt{2\pi}\sigma_g}\exp\left[\frac{-(\ln r - \ln r_g)^2}{2\sigma_g^2}\right]d\ln r \qquad (1)$$

where $(dn/dr)dr$ = number of particles per unit volume (concentration) having radii between r and $r + dr$, and N = total particle concentration, r_g = geometric mean radius, and σ_g = geometric standard deviation for each mode. The grand average of Table 2 in Whitby (1978), taken over a large number of observations, yields $r_g = 0.0065$ μm, $\sigma_g = 0.53$ for the NM, $r_g = 0.035$ μm, $\sigma_g = 0.7$ for the AM, and $r_g = 0.5$ μm, $\sigma_g = 0.8$ for the CM, where these values refer to the distribution by number. The corresponding values of geometric mean radius relative to the distribution by volume (or by mass if we assume a uniform density

Table 2. *Surface type characteristics used for CCM calculations with detailed surface physics parameterization; see Table 1 for the meaning of the various symbols*

Ref. no.	Surface type	Z_0 (cm)	Maximum fractional veg. cover, $F_{VG,summer}$	Seas. change in $F_{VG,summer}$
1	Crop	6	0.85	0.6
2	Short Grass	2	0.8	0.1
3	Evergreen Needle-leaf For.	100	0.8	0.1
4	Deciduous Needle-leaf For.	100	0.8	0.3
5	Deciduous Broadleaf For.	80	0.8	0.3
6	Evergreen Broadleaf For.	200	0.9	0.5
7	Tall Grass	10	0.8	0.3
8	Desert	5		
	Sea-ice	5		
9	Tundra	4	0.6	0.2
10	Irrigated Crop	6	0.8	0.6
11	Semi-desert	10	0.1	0.1
12	Ice-cap	1		
	Glacier	1		
13	Bog or Marsh	3	0.8	0.4
14	Inland Water†			
—	Ocean*			
16	Evergreen Shrub	10	0.8	0.2
17	Deciduous Shrub	10	0.8	0.3
18	Mixed Woodland	80	0.8	0.2

* See Table 1.
† Treated as ocean.

Table 2 *continued*

Ref. no.	Surface type	c_d	a (mm)	a_{sm} (μm)	A_{sm}	c_v/c_d	$C_{D_n}^{-1/2}$
1	Crop	0.3	1	10	10^{-4}	1/3	2.5
2	Short Grass	0.3	0.5	10	5×10^{-5}	1/3	2.5
3	Evergreen Needle-leaf For.	0.4	0.5	—	—	1/4	3
4	Deciduous Needle-leaf For.	0.4	0.5	—	—	1/4	3
5	Deciduous Broadleaf For.	0.4	10	10	10^{-4}	1/4	3
6	Evergreen Broadleaf For.	0.4	10	10	10^{-4}	1/4	3
7	Tall Grass	0.3	0.5	10	5×10^{-5}	1/3	2.5
8	Desert‡						
	Sea-ice‡						
9	Tundra	0.3	0.5	10	5×10^{-5}	1/3	2.5
10	Irrigated Crop	0.3	1	10	10^{-4}	1/3	2.5
11	Semi-desert	0.3	0.5	10	5×10^{-5}	1/3	2.5
12	Ice-cap‡						
	Glacier‡						
13	Bog or Marsh	0.3	0.5	10	5×10^{-5}	1/3	2.5
14	Inland Water†						
—	Ocean*						
16	Evergreen Shrub	0.4	0.5	—	—	1/4	2.5
17	Deciduous Shrub	0.4	10	10	10^{-4}	1/4	2.5
18	Mixed Woodland	0.4	0.5	—	—	1/4	3

* See Table 1.
† Treated as ocean.
‡ Treated as a surface with bluff roughness elements (see Table 1).

for the particles in a given mode) are 0.015 μm for the NM, 0.15 μm for the AM, and 3.4 μm for the CM. Here, number-average and mass-average deposition velocities, respectively V_N and V_M, will be calculated for the NM, AM, and CM, where

$$V_N = \frac{\int v_{dep}(r) \frac{dn(r)}{dr} dr}{\int \frac{dn(r)}{dr} dr},$$

$$V_M = \frac{\int \frac{4}{3} \pi v_{dep}(r) \rho_p r^3 \frac{dn(r)}{dr} dr}{\int \frac{4}{3} \pi \rho_p r^3 \frac{dn(r)}{dr} dr}. \tag{2}$$

In (2), v_{dep} is the particle deposition velocity calculated from (a)–(h) of Table 1, $(dn/dr)dr$ is given by (1), and ρ_p is the particle density, assumed to be equal to 1.5 g/cm^3 for the NM and AM, representative of particles with a large sulfate component, and 2.5 g/cm^3 for the CM, typical of dust particles (Whitby, 1978; Pruppacher and Klett, 1978). For r_g and σ_g the corresponding values mentioned above given by Whitby (1978) are used. Note that a specification of the total number concentration N appearing in (1) is not necessary since N appears in both the numerator and the denominator of (2). The integrals in (2) are calculated numerically.

Different versions of the Community Climate Model (CCM) of the National Center for Atmospheric Research (NCAR) will be used to generate the meteorological fields necessary for the computation of the particle deposition velocities. Since this GCM is extensively documented elsewhere (Williamson, 1983; Williamson and Williamson, 1984; Pitcher et al., 1983; Malone et al., 1984; Ramanathan et al., 1983), only descriptions of the surface layer processes that affect our calculations will be presented for each model used.

3. Global scale deposition velocities of ambient aerosols: GCM simulations with simple surface physics parameterization

In this section, calculations of particle deposition velocities are carried out using the standard version of the CCM under January conditions. In this version of the CCM the boundary layer processes that lead to surface exchanges of momentum, heat, and water vapor are parameterized using the well-known bulk formulas (e.g., Williamson, 1983)

$$\begin{aligned} \tau_\lambda &= -\rho_h C_D U_h U_{\lambda h}, \\ \tau_\mu &= -\rho_h C_D U_h U_{\mu h}, \\ H_T &= c_p \rho_h C_D U_h \left(T_s - \frac{T_h}{\sigma_h^{k_g}} \right), \\ W &= D_w \rho_h C_D U_h (q_s(T_s) - q_h), \end{aligned} \tag{3}$$

where the subscript h refers to the bottom model level and U_h = magnitude of the wind, $U_{\lambda h}$ and $U_{\mu h}$ = eastward and northward components of the wind, respectively, ρ_h = air's density, C_D = surface drag coefficient, T_h = air temperature, T_s = surface temperature, c_p = specific heat at constant pressure, $k_g = R_g/c_p$ with R_g = gas constant for dry air, $\sigma_h = p_h/p_s$, where p = pressure and p_s = surface pressure, D_w = surface wetness factor, q_h = specific humidity, q_s = specific humidity at the surface, and τ_λ, τ_μ = surface fluxes of the eastward and northward components of momentum, H_T = surface heat flux, and W = surface water vapor flux. The height h of the bottom CCM level is about 70 m.

The parameter needed from (3) for the particle deposition calculations is the surface drag coefficient C_D. Only three types of surfaces are defined in this version of the CCM, with corresponding prescribed constant values of C_D: ocean with $C_D = 10^{-3}$; snow and sea ice with $C_D = 10^{-3}$; land with $C_D = 4 \times 10^{-3}$. The distribution of land, snow, sea ice, and ocean surfaces is prescribed. Snow and sea ice areas can be identified approximately by land and sea areas north of a latitude of about 45°N and south of a latitude of about 65°S. Snow and sea ice are treated in the fully rough regime as surfaces with bluff roughness elements having a roughness length of 0.03 cm (Brown, 1981). The land surface is assumed to be covered by an "average" canopy characterized by a "large collector" radius $a = 0.5$ mm, a "small collector" radius $a_{sm} = 10$ μm, a value of the parameter $A_{sm} = 5 \times 10^{-5}$, $c_v/c_d = 1/3$, $c_d = 0.3$, and $C_{D_0}^{-1/2} = 2.5$ (see Table 1 and GI). The choice of these parameters gives deposition velocities roughly characteristic of grass fields (see Fig. 2).

Fig. 3 first shows an example of snapshots of the calculated mass deposition velocity fields for typical model-produced conditions in the absence of the diffusiophoretic effect over ocean. Also

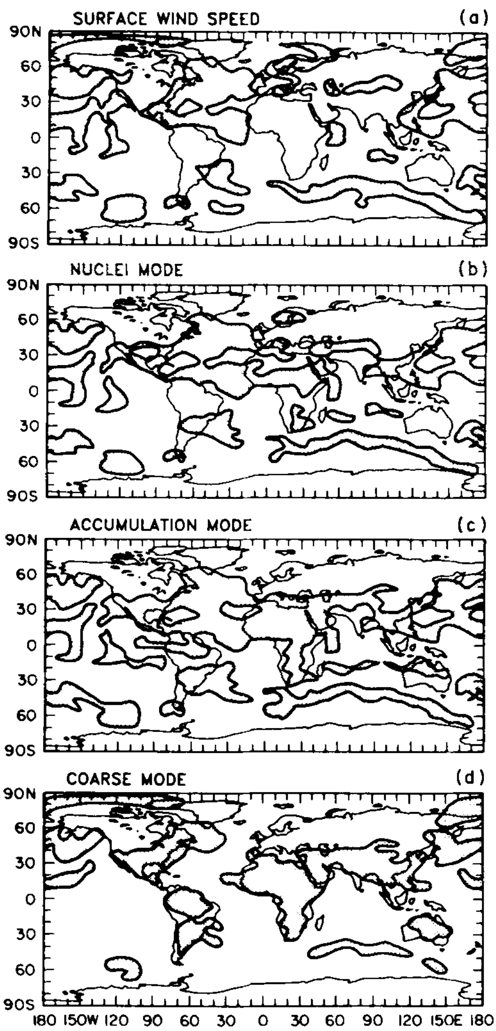

Fig. 3. Surface wind speed U_h, and aerosol mass-average deposition velocity V_M, standard CCM, January conditions, day 15. (a), U_h, shaded areas $\rightarrow 10 \leqslant U_h \leqslant 21$ m/s, elsewhere $U_h < 10$ m/s. (b), V_M, nuclei mode, shaded areas $\rightarrow 0.07 \leqslant V_M \leqslant 0.2$ cm/s, elsewhere $V_M < 0.07$ cm/s. (c), V_M, accumulation mode, shaded areas $\rightarrow 0.012 \leqslant V_M \leqslant 0.03$ cm/s, elsewhere $V_M < 0.012$ cm/s. (d), V_M, coarse mode, shaded areas $\rightarrow 1.8 \leqslant V_M \leqslant 3.5$ cm/s, elsewhere $V_M < 1.8$ cm/s.

shown is the corresponding surface wind speed field. The calculated V_M are in the range of 0.01–0.2 cm/s for the NM, 0.001–0.03 cm/s for the AM, and 1.25–3.5 cm/s for the CM. Correspondingly, the values of V_N (which are not reported since they present a similar spatial distribution) are 0.04–0.5 cm/s for the NM, 0.003–0.08 cm/s for the AM, and 0.02–0.4 for the CM. The bulk deposition velocities can thus vary considerably for different particle size distributions and for different moments of the distribution. A strong dependence of V_M on the surface wind speed is observed (hereafter the notation "surface wind speed" will indicate "wind speed at the height h of the lowest model level"), implying that the spatial and temporal variability of the deposition will to some extent correlate with the surface wind speed variability. Also, particularly for the AM and the CM, particle deposition seems to be significantly sensitive to the surface type, as indicated by the presence of high deposition velocities over land even in regions of low wind speed. This is better illustrated in Fig. 4, which shows deposition velocities and wind speeds averaged over a 20-day simulation.

Two features are of particular interest. First, the values of the mass deposition velocity remain in the fairly well defined range (after averaging) of 0.015–0.12 cm/s for the NM, 0.002–0.024 cm/s for the AM, and 1.25–3 cm/s for the CM. Second, in addition to the already mentioned wind speed dependence (more evident over ocean), we notice that all modes have deposition velocities that are on average higher over "land" than over snow, sea ice, and ocean surfaces. This difference, about a factor of 1.5–3, becomes more pronounced as the particle mode radius increases, due to the effect of impaction.

The combined wind- and surface-type dependence is also revealed by the time and zonally averaged deposition velocities of Fig. 5. The distribution of the peaks in the V_M field matches the peak structure in the surface wind speed field (note how the surface midlatitude westerlies and subtropical easterlies appear in Fig. 5), but the magnitude of the peaks is modulated by the amount of land present in the corresponding zonal bands. For each mode the deposition velocity presents relative maxima in the midlatitude and subtropical belts (higher in the northern hemisphere) and relative minima in the equa-

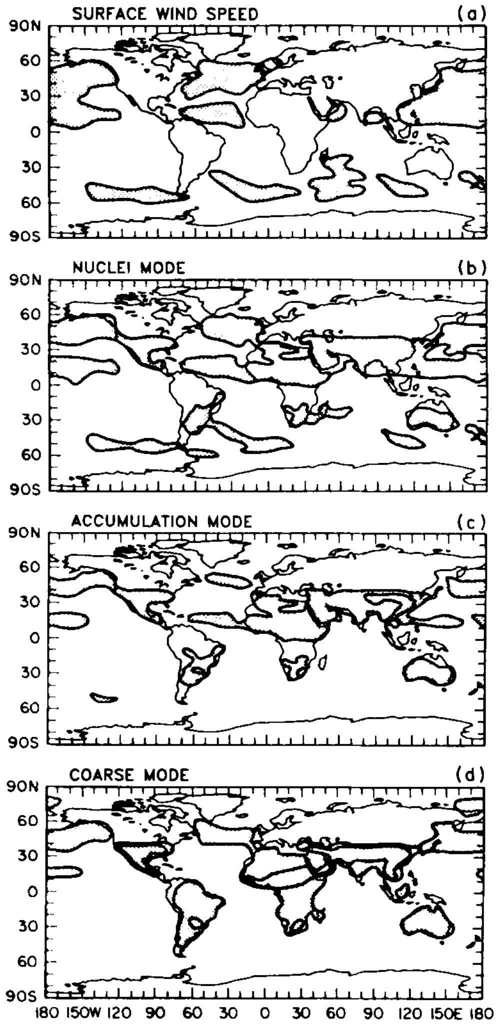

Fig. 4. Surface wind speed U_h, and aerosol mass-average deposition velocity V_M, standard CCM, January conditions, time-average, days 0–20. (a), U_h, shaded areas → $10 \leqslant U_h \leqslant 17$ m/s, elsewhere $U_h < 10$ m/s. (b), V_M, nuclei mode, shaded areas → $0.06 \leqslant V_M \leqslant 0.12$ cm/s, elsewhere $V_M < 0.06$ cm/s. (c), V_M, accumulation mode, shaded areas → $0.012 \leqslant V_M \leqslant 0.024$ cm/s, elsewhere $V_M < 0.012$ cm/s. Also shown is the 0.018 cm/s isoline. (d), V_M, coarse mode, shaded areas → $1.8 \leqslant V_M \leqslant 3$ cm/s, elsewhere $V_M < 1.8$ cm/s. Also shown is the 2.4 cm/s isoline.

torial, tropical, and polar regions. Interestingly, this trend is generally observed also in individual zonally averaged snapshots.

Thus, while the deposition velocity can be locally highly variable depending on the surface wind conditions, long-term averaged trends in the deposition velocity patterns are definitely observed, which are affected by particle size distribution, wind fields, and surface characteristics. Note that, since a single value of C_D (corresponding to a roughness length of approximately 10 cm) is used for all "land" areas, the particle deposition patterns over snow-free continental regions are related to the corresponding surface wind-speed patterns. The dependence of the deposition velocity on the characteristics of different land types will be examined in the next section.

Some authors in the past have speculated that the surface diffusiophoretic effect induced by water vapor evaporation and condensation could be relevant for deposition over ocean (Slinn, 1977; Slinn and Slinn, 1980; Slinn et al., 1978). It thus seemed interesting to estimate this effect on a global scale with the present model by introducing a diffusiophoretic drift velocity as given in Table 1.

The effect of diffusiophoresis is illustrated in Fig. 6 where AM time-averaged deposition velocities are reported. The model-produced diffusiophoretic drift velocities generally varied in the range of -0.015–0.001 cm/s, the inhibiting action of evaporation (negative drift velocities) being strongly dominant. The effect associated with evaporation is especially noticeable in the tropical and equatorial regions where deposition of AM particles is strongly inhibited. In these regions the calculated deposition velocities become less than 5×10^{-5} cm/s. Since the diffusiophoretic drift velocity is size-independent, the effect on NM and CM deposition is relatively less important. Nevertheless, if the formula of Table 1 can be considered valid for field conditions, this example shows that for the long-lived background aerosol, diffusiophoresis plays a significant rôle in slowing deposition over the ocean.

Another issue often discussed in the literature is the effect of growth of soluble particles due to condensation of water vapor at the high relative humidities near the ocean-air interface. Slinn and Slinn (1980) hypothesized that particle growth could considerably enhance the deposition of submicron particles. However, in a recent work, Jenkin (1984) has shown that this effect is not larger than the uncertainty present in measured,

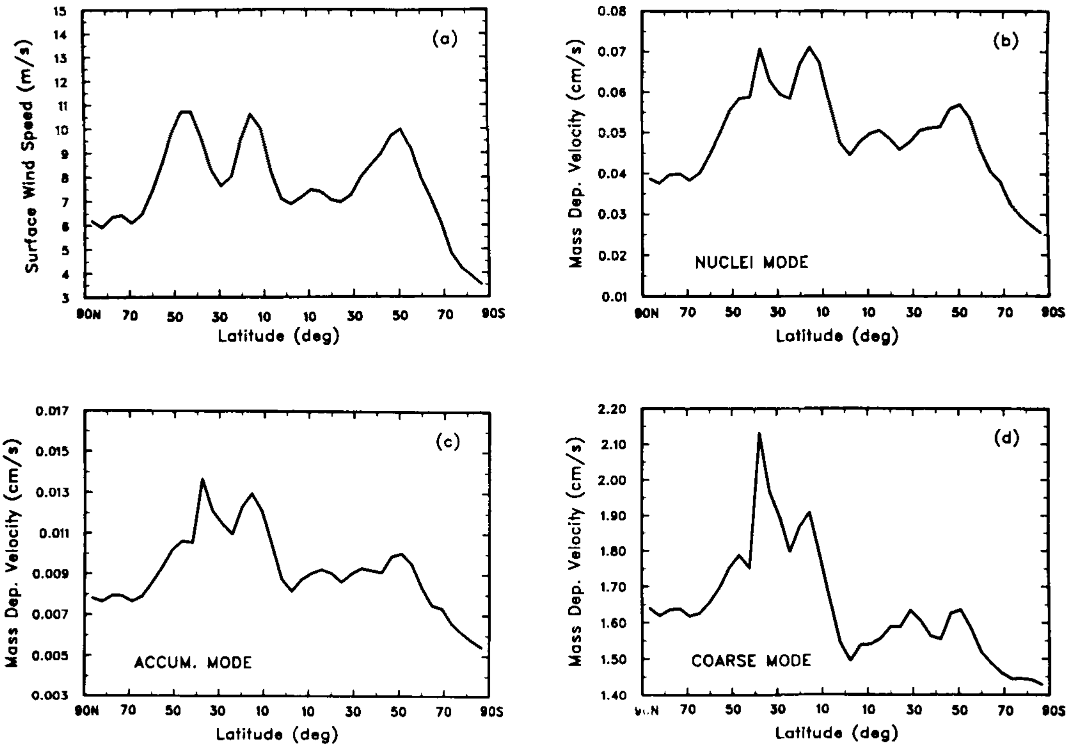

Fig. 5. Time- and zonally averaged (days 0–20) surface wind speed U_h (Fig. 5a) and mass-average deposition velocity for NM, AM, and CM (Figs. 5b, c, d, respectively), standard CCM, January conditions.

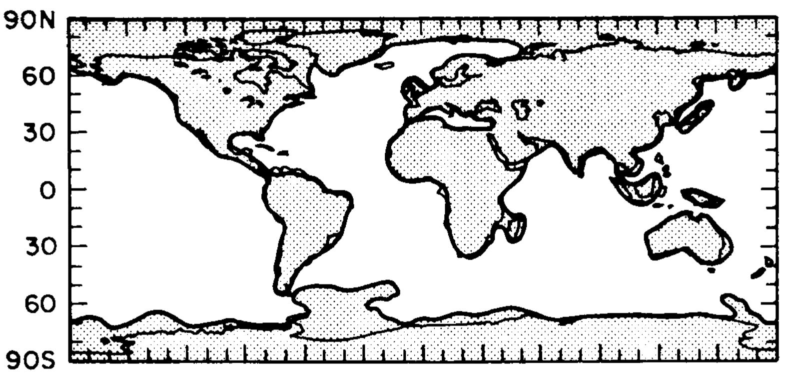

Fig. 6. Accumulation mode mass-average deposition velocity V_M, calculated including the diffusiophoretic effect over the ocean surface, standard CCM, January conditions, time-average, days 0–20. Shaded areas → $V_M \geq 0.005$ cm/s, elsewhere $V_M < 0.005$ cm/s.

and probably model-derived, deposition velocities. It is nevertheless interesting to estimate what its influence would be on our simulated particle deposition.

For this purpose, the growth model of Slinn and Slinn (1980) can be used. In this model a "wet" particle radius is used in place of the dry radius in the expression of interfacial layer transfer velocity and gravitational settling velocity at the height δ. The wet radius is obtained using the formulas of Fitzgerald (1975) under the assumption that the particle is in equilibrium at the relative humidity near the water interface. The general validity of this assumption has been criticized on the basis of comparisons of typical particle residence times near the surface and characteristic particle growth times (e.g., Ferron, 1977; Jenkin, 1984). The equilibrium assumption seems to be valid only for very small particles that very rapidly reach the equilibrium size; for this reason only results from calculations for the NM and the AM will be reported here.

The other major uncertainty of this model concerns the value of relative humidity for use in the equilibrium radius calculations. The relative humidity at the air-ocean interface is equal to about 98.2% because of the presence of dissolved salts (e.g., Williams, 1982). On the other hand, since the relative humidity in the interfacial laminar sublayer drops rapidly away from the interface, Jenkin (1984) and Garland (1983) suggest that a more suitable range would be 90–95%. Here, in order to estimate an upper limit of the particle growth effect over ocean, the value of 98% will be used in the context of Slinn and Slinn's model.

With this assumption, mass deposition velocities over ocean surfaces were recalculated for 100% ammonium sulfate NM and AM particles. For these particles the equilibrium radius growth at 98% relative humidity is about a factor of 3. While the deposition spatial and temporal patterns remained basically unchanged, the values of V_M decreased by a factor of about 2 for the NM and changed only slightly for the AM. Note that these variations would be even less pronounced when using relative humidities of 90–95% in the wet radii calculations. This result can be understood when noting that for the NM, and to a lesser extent the AM, most of the particles lie in a region of the size spectrum where an increase in size of the order of that produced by equilibrium growth at 98% relative humidity results in a decrease in the corresponding deposition velocity (see Fig. 1).

Although the growth model employed to derive these estimates is affected by a high degree of uncertainty, these calculations show that for observed ambient aerosol size distributions the effect of particle growth probably represents only a minor contribution to the overall deposition rate, at this stage well within the range of uncertainty present in current modeling of particle deposition over the ocean surface.

In summary, the calculations presented in this section show a quite intriguing pattern of dependencies of the aerosol deposition velocities upon particle properties, wind speed, and surface characteristics. However, highly parameterized surface physics was employed in these simulations, along with a very limited number of surface types. It is thus necessary to evaluate how sensitive the calculated deposition velocities are to a more accurate treatment of the boundary layer and to a more detailed specification of the land type distribution. This problem will be addressed in the next section.

4. Global scale deposition velocities of ambient aerosols: GCM simulations with a more detailed surface physics parameterization

In this section, global scale deposition velocities are calculated using a version of the CCM containing a more detailed description of surface physics. The new boundary layer parameterization package has been developed by various members of the Atmospheric Analysis and Prediction Division of NCAR and other collaborators, and is described in detail in Dickinson et al. (1981, 1987), and Dickinson (1984).

Many innovations are of interest for our calculations. Briefly, 18 land-surface types are defined in the standard CCM horizontal resolution (approximately 5° latitude and 7.5° longitude), based upon the land-use data archives of Matthews (1983, 1984), Wilson (1984), Wilson and Henderson-Sellers (1985), and Henderson-Sellers et al. (1986) (see Table 2 and Fig. 7). At each land grid point, depending on surface type assignment, season, and surface temperature, a fraction of the grid point covered by vegetation F_{VG} is defined, the remaining fraction $F_{BS} = 1 - F_{VG}$ being assumed to be covered by bare soil. Referring to Table 2, F_{VG} varies roughly as a quadratic function of the model subsoil temperature T_{g2} (see below) from $F_{VG,summer}$ if $T_{g2} > 298$ k to $F_{VG,summer} - \Delta F_{VG}$ if $T_{g2} < 273$ k,

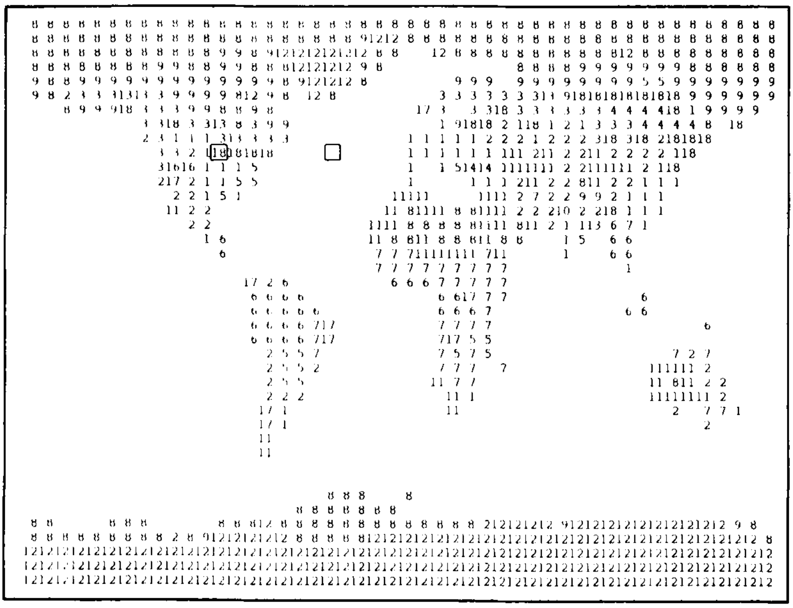

Fig. 7. Surface land-type distribution for the CCM with detailed surface physics parameterization (see Table 2 for the meaning of the various surface type reference numbers). Also indicated are the grid points relative to Figs. 8–10.

where ΔF_{VG} is the seasonal change in F_{VG} (Dickinson et al., in press). Fractions of snow cover for both vegetation and bare soil, respectively F_{SVG} and F_{SBS}, are then diagnostically calculated depending on the local temperature and precipitation type.

Over land, surface exchanges of momentum, sensible heat, and water vapor are calculated via a bulk parameterization that makes use of a "transfer resistance" model including (a) a turbulent atmospheric layer extending from the bottom CCM level h (again, of about 70 m height) to the top of the canopy, or to the bare ground, in which turbulent transport also depends on the atmospheric stability; (b) a canopy layer (in presence of vegetation) in which the transfer rate depends on the characteristics and leaf area index of the vegetation elements; and (c) a diffusive (soil or snow) layer consisting of a surface ground sublayer of about 10 cm depth and a subsoil sublayer typically of a few meters depth. The temperatures within the canopy, of foliage elements, of the top ground layer, and of the subsoil layer are calculated via energy balance considerations. Over oceans, the temperature is seasonally prescribed, and exchanges of momentum, sensible heat, and water vapor are calculated via relations such as (3).

The hydrologic cycle is also represented in great detail. The processes included are precipitation (in the form of rain or snow depending on the temperature in the bottom model level), interception of rain by foliage, plant transpiration, evaporation (or sublimation) from the soil, infiltration and percolation to groundwater, surface runoff, and water phase changes in the soil layer. The model also includes the seasonal as well as the diurnal cycle.

Since in our particle deposition scheme the surface is treated as a perfect sink (i.e., having zero resistance to particle transfer), the quantities needed for the deposition calculations from the new boundary layer package are (a) characterizations of the surface types; (b) momentum drag coefficient (which parameterizes the bulk transfer in the turbulent atmospheric layer); and (c) fraction of the grid point occupied by soil (or water), vegetation, and snow. Table 2 presents for each surface type the values assumed here for the relevant quantities appearing in the deposition velocity calculations (see Table 1). These values, particularly for quantities such as the large collector radius a and the parameter A_{sm}, are admittedly only tentative and have been chosen mainly for illustrative purposes.

The drag coefficient C_D is calculated (Dickinson et al., in press) as a function of C_{DN}, the drag coefficient for neutral stability, and the surface bulk Richardson number

$$\mathrm{Ri_B} = \frac{gh(1 - T_g/T_h)}{U_0^2} \tag{4}$$

where $U_0^2 = U_{\lambda h}^2 + U_{\mu h}^2 + U_c^2$, T_g = top ground (or snow and sea ice) temperature, T_h, $U_{\lambda h}$, $U_{\mu h}$ = air (potential) temperature, and eastward and northward components of the wind at the height of the lowest model level h, and U_c, the convective wind speed, is given by

$$\begin{aligned} U_c &= 0.1 \text{ m/s}, \quad T_h/T_g \geq 1 \\ U_c &= 1.0 \text{ m/s}, \quad T_g/T_h \geq 1. \end{aligned} \tag{5}$$

In the presence of vegetation, the air temperature within the canopy is used in (4) in place of T_g.

With these definitions, C_D is assumed to be equal, for $\mathrm{Ri_B} \leq 0$, to

$$C_D = C_{DN}(1 + 24.5(-C_{DN}\,\mathrm{Ri_B})^{1/2}) \tag{6}$$

and for $\mathrm{Ri_B} \geq 0$ to

$$C_D = C_{DN}/(1 + 11.5\mathrm{Ri_B}). \tag{7}$$

Eqs. (6) and (7) are a slight modification of formulae given in some notes of Deardoff (see Dickinson, 1981, 1987). For heat transfer the same values of C_D are used, even though in reality the value for heat is somewhat larger for unstable conditions and somewhat smaller for stable conditions. As explained in Dickinson (1981, 1987), "This refinement did not seem to be numerically large enough to warrant its inclusion."

The neutral drag coefficient is given by

$$C_{DN} = \left[\frac{\kappa}{\ln(h/Z_0)}\right]^2. \tag{8}$$

where κ is the von Karman constant, equal to 0.4, and Z_0 is the roughness length. For water surfaces it is assumed that the neutral drag coefficient relative to a height of 10 m is equal to 0.0014, which gives from (8) an average value of $Z_0 = 2.3 \times 10^{-4}$ m. For bare soil Z_0 is taken to be equal to 10^{-2} m and for snow $Z_0 = 3 \times 10^{-4}$ m. After the stability correction the drag coefficient is lower bounded by the value 4×10^{-4}.

Given these model-produced parameters, at each grid point the deposition velocity is calculated as

$$v_{dep} = F_{BS}v_{BS} + F_{VG}v_{VG} + F_{SN}v_{SN}, \tag{9}$$

where F_{BS}, F_{VG}, and F_{SN} ($= F_{SVG} + F_{SBS}$) are the fraction of grid point occupied respectively by bare soil (or water), vegetation, and snow (or sea ice), and v_{BS}, v_{VG}, and v_{SN} the corresponding deposition velocities derived from the formulas in Table 1. Eq. (9) is then used in (2) to calculate the mass deposition velocity V_M.

For these calculations U_0 as defined in (4) is used in (a)–(h) of Table 1 in place of the wind speed at the bottom CCM level U_h. The addition of a convective velocity to U_h prevents the particle turbulent deposition rate from vanishing when the calculated surface wind speed is equal to 0. Note that in grid points composed of different types of surfaces (for example, vegetation and bare soil, or vegetation, bare soil, and snow), the same value of surface wind speed and bulk Richardson number are used to calculate the corresponding deposition velocities. As shown by Walcek et al. (1986), this procedure may somewhat overestimate the computed averaged deposition velocities; however, its use was motivated by consistency with the momentum transfer calculations in the host model.

Simulations have been carried out using the CCM with the new boundary layer package for both January and July conditions. Figs. 8, 9, and 10 first show the temporal variation of relevant aerodynamic parameters and mass deposition velocity for the various aerosol modes at two grid points, for July and January simulations. Figs. 8 and 10 refer to a grid point located in the midcontinental United States characterized by vegetation type 18 (mixed woodland), while Fig. 9 refers to a grid point in the Northern Hemisphere Atlantic Ocean (see Fig. 7).

Fig. 8 emphasizes the effect of the diurnal cycle on the deposition velocities calculated over land areas when the mean solar zenith angle is relatively small (i.e., in conditions of maximum insolation). During daylight hours, as indicated by a sharp decrease in bulk Richardson number, the insolation increases the surface temperature and, as a consequence, the convective instability near the surface. As indicated by the friction velocity trend, this enhances turbulent transport

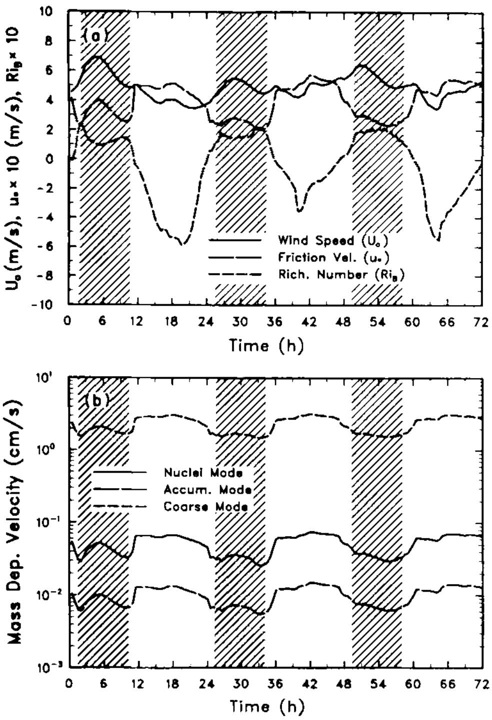

Fig. 8. Richardson number, surface wind speed U_0, friction velocity, and mass-average deposition velocities for NM, AM, and CM as a function of time over a continental United States grid point (see Fig. 7); July conditions. Shaded areas indicate nighttime conditions.

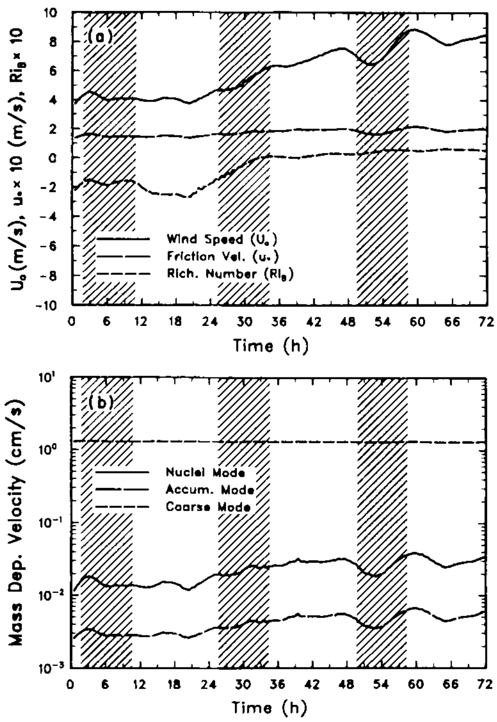

Fig. 9. Richardson number, surface wind speed U_0, friction velocity, and mass-average deposition velocities for NM, AM, and CM as a function of time over a northern hemisphere Atlantic Ocean grid point (see Fig. 7); July conditions. Shaded areas indicate nighttime conditions.

through the boundary layer and in turn the particle deposition velocity. For all modes, deposition is in fact more efficient during daytime than during nighttime on average by a factor of about 1.5–2.5, and is mostly correlated with the friction velocity. Interestingly, the higher wind speeds associated with nighttime conditions tend to somewhat compensate for the effect of the convective stability trend.

As shown in Fig. 9, the situation over ocean is quite different. Because of the high heat capacity of water, simulated in the model by prescribing a seasonal ocean surface temperature, the influence of the diurnal cycle becomes much less important (the Richardson number's temporal trend is basically determined by large scale temperature advection), and the dependence on wind speed dominates for the NM and AM. For the CM, at the simulated low surface-wind speeds over this grid point, the contribution of gravitational settling is largely dominant. At higher wind speeds, due to the enhanced efficiency of impaction, the wind speed dependence for the CM becomes more evident (see below).

Finally, Fig. 10 refers to the same land grid point of Fig. 8, except for a January simulation, i.e., in conditions of high mean solar zenith angle and lower insolation. In this case, as expected, the diurnal cycle is much less evident than it is for summer conditions, and the effect of synoptic systems is more important. The boundary layer is generally more stable, and the surface wind speed dependence is accentuated.

A similar analysis was also carried out for grid points at different locations, corresponding to different surface types, and the results showed a behavior similar to that indicated in Figs. 8–10.

The dependence of the mass deposition velocity on the surface type is revealed by Figs. 11

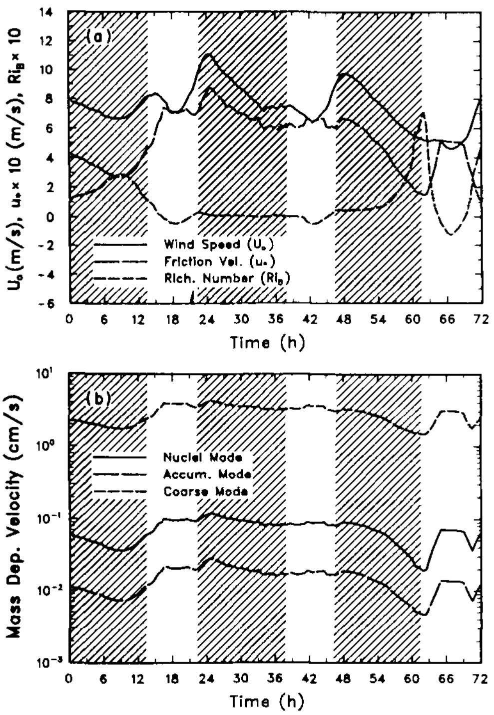

Fig. 10. Richardson number, surface wind speed U_0, friction velocity, and mass-average deposition velocities for NM, AM, and CM as a function of time over a continental United States grid point (see Fig. 7); January conditions. Shaded areas indicate nighttime conditions.

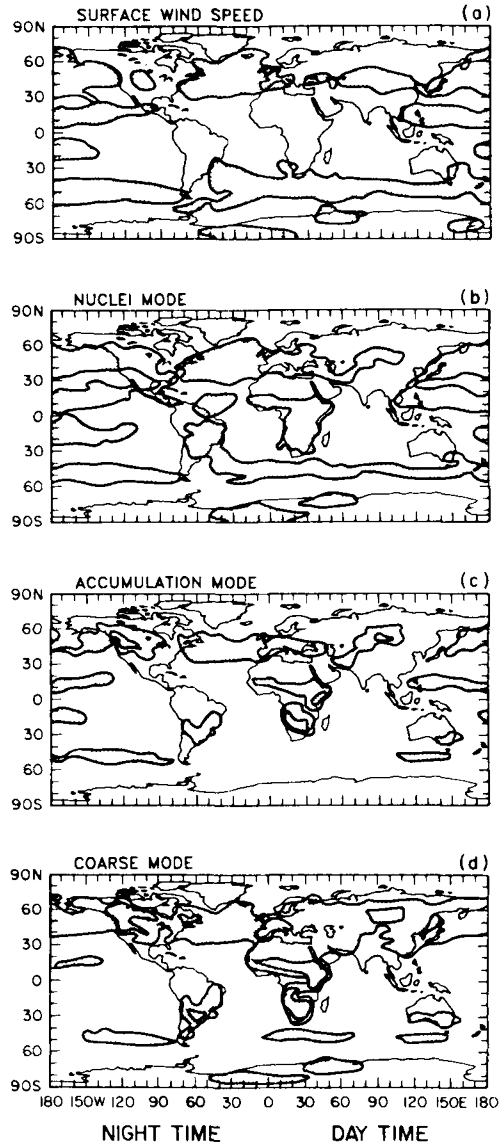

Fig. 11. Surface wind speed U_0, and aerosol mass-average deposition velocity V_M, CCM with detailed surface physics parameterization, January conditions, time-average over 18.00 GMT snapshots, days 0–20. Daytime and nighttime areas are roughly indicated. (a), U_0, shaded areas → $10 \leqslant U_0 \leqslant 19$ m/s, elsewhere $U_0 < 10$ m/s. (b), V_M, nuclei mode, shaded areas → $0.06 \leqslant V_M \leqslant 0.15$ cm/s, elsewhere $V_M < 0.06$ cm/s. (c), V_M, accumulation mode, shaded areas → $0.012 \leqslant V_M \leqslant 0.025$ cm/s, elsewhere $V_M < 0.012$ cm/s. Also shown is the 0.018 cm/s isoline. (d), V_M, coarse mode, shaded areas → $1.8 \leqslant V_M \leqslant 3.5$ cm/s, elsewhere $V_M < 1.8$ cm/s. Also shown is the 2.4 cm/s isoline.

and 12, which show surface wind speed and deposition velocity for the three modes over the entire domain averaged over 20-day simulations. Because of the dependence of the results on the diurnal cycle the averages were taken using snapshots corresponding to the same time of the day, namely 18.00 GMT. Areas roughly corresponding to night- and daytime are indicated in the figure.

Averaged deposition velocities over ocean lie in the same range as for the standard CCM simulations and show a similar wind speed dependence. On the other hand, deposition over land presents some interesting features. With reference to the land type distribution of Fig. 7, it can first be noted that, for each mode, deposition velocities over vegetated areas are higher than over desert, semidesert, and snow-covered (or sea ice) areas by a factor of 1.5–3. This difference becomes more pronounced for the AM and CM

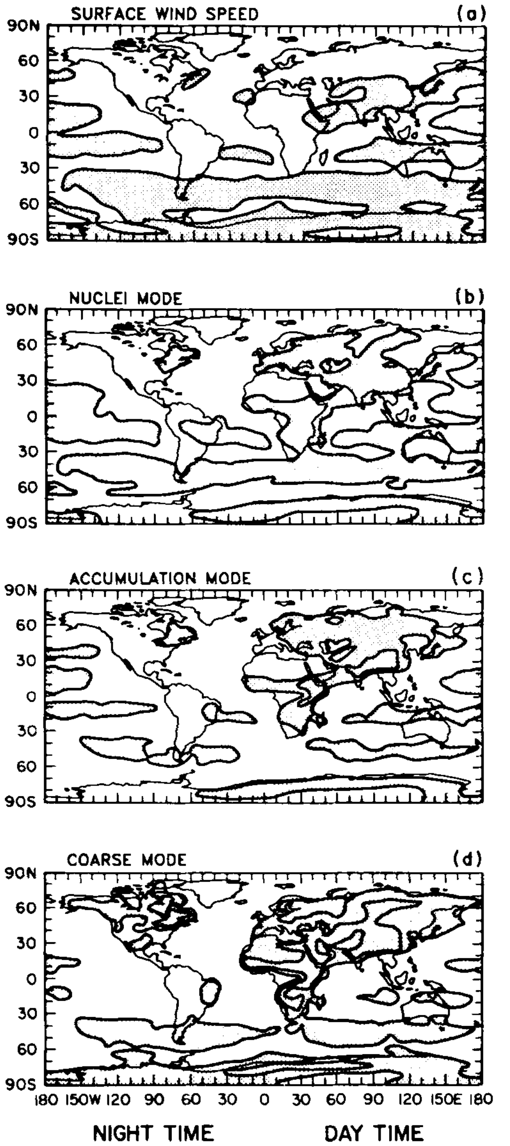

Fig. 12. Surface wind speed U_0, and aerosol mass-average deposition velocity V_M, CCM with detailed surface physics parameterization, July conditions, time-average over 18.00 GMT snapshots, days 0–20. Daytime and nighttime areas are roughly indicated. (a), U_0, shaded areas $\rightarrow 10 \leqslant U_0 \leqslant 19$ m/s, elsewhere $U_0 < 10$ m/s. (b), V_M, nuclei mode, shaded areas $\rightarrow 0.06 \leqslant V_M \leqslant 0.15$ cm/s, elsewhere $V_M < 0.06$ cm/s. (c), V_M, accumulation mode, shaded areas $\rightarrow 0.012 \leqslant V_M \leqslant 0.03$ cm/s, elsewhere $V_M < 0.012$ cm/s. Also shown is the 0.018 cm/s isoline. (d), V_M, coarse mode, shaded areas $\rightarrow 1.8 \leqslant V_M \leqslant 3.5$ cm/s, elsewhere $V_M < 1.8$ cm/s. Also shown is the 2.4 cm/s isoline.

due to the increasing efficiency of interception and impaction. For the AM and CM there also seem to be detectable differences in the large scale deposition efficiencies over different vegetation types. Note, for example, the relatively higher deposition velocities (up to averaged values of 0.03 cm/s for the AM and 3.5 cm/s for the CM, and instantaneous values of 0.05 cm/s for the AM and 5 cm/s for the CM) over needleleaf forests and tall grass due to the high collection efficiency of the vegetative collectors. Conversely, relatively lower values are calculated over broadleaf forests due to a combination of low collection efficiency and low averaged surface wind speeds. Deposition rates over other vegetation types lie between these two limits. For the NM, the deposition velocity over vegetation appears to be more uniform, lying in the range of 0.015–0.15 cm/s.

Seasonal effects can be deduced by comparing Figs. 11 and 12. The surface wind speed, and so the deposition velocity, is generally larger in the winter hemisphere midlatitudes, particularly over oceans. Over land, the surface vegetation type and the diurnal cycle dependencies play the most important rôle as indicated by the generally higher deposition velocities over vegetated, daytime (at small mean solar zenith angle) areas. Seasonal differences on a regional scale can be noticed (for example in the Northwestern United States and Canada and areas of continental Asia), being related to the interactions of seasonal surface wind speed and insolation patterns.

The time and zonally averaged deposition velocity profiles (Fig. 13) show characteristics similar to those obtained with the simple boundary layer simulations. A similar pattern of "modulated" peaks is in fact found, corresponding to the wind speed peak distribution, the main modulation factor being in this case the fractional vegetation cover in a latitudinal band in place of the fractional land cover. Relative maxima are, again, roughly located in the midlatitude and subtropical belts, with deposition velocities generally increasing in the winter hemispheres.

In summary, although of a rather crude and somewhat tentative nature, the deposition calculations presented in this section emphasize, in addition to the already investigated wind speed dependence of the deposition rates, the following

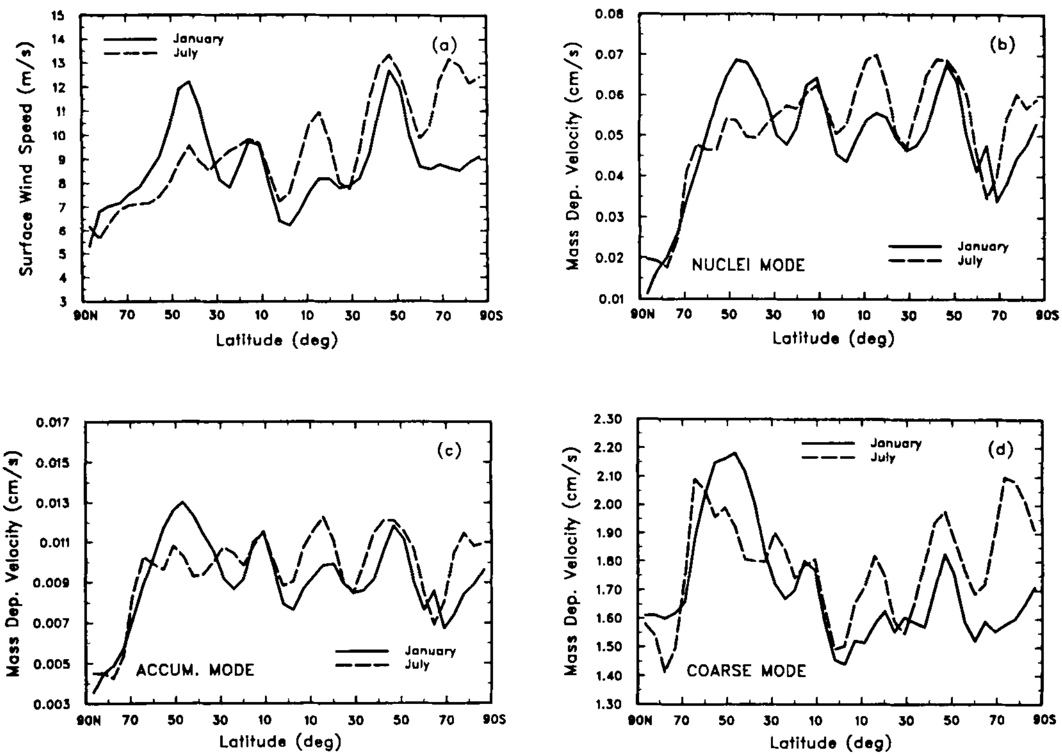

Fig. 13. Time- and zonally averaged (over 18.00 GMT snapshots, days 0–20) surface wind speed U_0 (Fig. 13a) and mass-average deposition velocity for NM, AM, and CM (Figs. 13b, c, d, respectively), CCM with detailed surface physics parameterization.

two effects: (a) The diurnal cycle affects the particle deposition patterns over land, especially for small mean solar zenith angle conditions, in that it influences the convective stability near the surface and thus the turbulent transfer through the boundary layer; and (b) deposition is more efficient over vegetated areas than over bare soil or snow fields, and can significantly vary from one vegetation type to the other. Thus, the use of diurnal and/or land-use-type averaged deposition velocity over land may lead to significant errors in simulating global ambient aerosol deposition rates.

5. Conclusion

In this work the semiempirical dry deposition parameterization scheme described by Giorgi (1986) has been applied to a general circulation model to study global scale deposition velocities of ambient aerosols assuming no shifts of particle size distribution with location. This study has first of all effectively illustrated the versatility of this dry deposition parameterization scheme, which has been applied to a number of case studies including deposition over a variety of surface types, effects of various meteorological variables, and relative importance of different deposition mechanisms.

The calculations presented here show that large scale dry deposition velocities are highly variable in space and time, this variability being sensitive in a complex fashion to local meteorological conditions near the surface (wind speed and atmospheric convective stability), surface characteristics (surface roughness length and properties of the roughness elements), and particle properties (particle radius and density). Since this variability can affect the deposition patterns of atmospheric pollutants, it should in some way be accounted for in models of atmospheric aerosol cycling. Calculated mass deposition velocities for the continental aerosol nuclei, accumulation, and coarse modes are less than about 0.2 cm/s, 0.05 cm/s, and 5 cm/s for individual snapshots, and 0.15 cm/s, 0.03 cm/s, and 3.5 cm/s when averaging over long-term simulations, respectively. They are higher on average over vegetated areas than over bare soil, ocean, snow, and sea ice by a factor varying from 1.5 to 3, can significantly depend on the vegetation type, and increase with wind speed and boundary layer convective instability. The diurnal cycle is here found to have an important effect on the deposition rates over land areas, particularly for high insolation (i.e., small mean solar zenith angle) conditions. The deposition velocities are in fact higher during daytime than during nighttime by a factor of 1.5–2.5 depending on insolation. Following the surface wind speed and land distribution patterns, zonally averaged deposition velocities show relative maxima in the midlatitude and subtropical belts, generally more pronounced in the winter hemispheres. It was also found that diffusiophoresis over evaporating ocean surfaces may be significant in inhibiting deposition of accumulation-mode particles.

As already pointed out, our calculations are only tentative in many aspects, particularly in the extension of a semiempirically based description of dry deposition to field conditions, and as such should be viewed as preliminary and illustrative. Future studies should also investigate the analog with heat (rather than momentum) transfer to the surface, and the changes in dry deposition velocities caused by the evolution in the particle size distribution due to microphysical processes. Measurements of particle deposition in which relevant meteorological and microphysical variables are carefully monitored are needed, both in the laboratory and in the field, to narrow the uncertainty that exists today in estimates of atmospheric aerosol residence times.

6. Acknowledgements

I am indebted to Robert Dickinson for providing the detailed boundary layer package employed for some of the calculations presented in this work and for his suggestions on the manuscript. I would also like to thank Christopher Walcek and the anonymous reviewers for their comments and insights on the paper.

REFERENCES

Bondietti, E. A., Hoffmann, F. O. and Larsen, I. L. 1984. Air-to-vegetation transfer rates of natural submicron aerosols. *J. Environ. Radioact. 1*, 5–27.

Brown, R. A. 1981. Modelling of the geostrophic drag coefficient for AIDJEX. *J. Geophys. Res. 86*, 1989–1994.

Chamberlain, A. C. 1967. Transport of Lycopodium spores and other small particles to rough surfaces. *Proc. Roy. Soc. A 296*, 45–70.

Dickinson, R. E. 1984. Modeling evapotranspiration for three-dimensional global climate models, in Climate processes and climate sensitivity, *Geophysical Monograph 29*, 58–72.

Dickinson, R. E., Jager, J., Washington, W. M. and Wolski, R. 1981. Boundary subroutine for the NCAR global climate model, NCAR Technical Note, NCAR/TN-173+1A.

Dickinson, R. E., Kennedy, P. J., Henderson-Sellers, A. and Wilson, M. 1987. Biosphere-Atmosphere Transfer Scheme (BATS) for the NCAR Community Climate Model, NCAR Technical Note.

Ferron, G. A. 1977. The size of soluble aerosol particles as a function of the humidity of the air. Application to the human respiratory tract. *J. Aerosol Sci. 8*, 251–267.

Fitzgerald, J. W. 1975. Approximate formulas for the equilibrium size of an aerosol particle as a function of its dry size and composition and the ambient relative humidity. *J. Appl. Meteorol. 14*, 1044–1049.

Garland, J. A. 1983. Dry deposition to grass in field conditions. In: *Precipitation, Dry Deposition, and Resuspension* (eds. H. R. Pruppacher, R. G. Semonin, and W. G. N. Slinn). Elsevier, New York, 731–751.

Giorgi, F. 1986. A particle dry deposition parameterization scheme for use in tracer transport models. *J. Geophys. Res. 91*, 9794–9806.

Henderson-Sellers, A., Wilson, M. F., Thomas, G. and Dickinson, R. E. 1986. Current global land-surface data sets for use in climate-related studies. NCAR Technical Note, NCAR/TN-272+STR.

Jenkin, M. E. 1984. An investigation into the enhancement of deposition of hygroscopic aerosols to wet surfaces in a wind tunnel. *Atmos. Environ. 18*, 1017–1024.

Jonas, R. and Heinemann, K. 1985. Studies of the dry deposition of aerosol particles on vegetation and plane surfaces. *J. Aerosol Sci. 16*, 463–471.

Lindberg, S. E., Harriss, R. C. and Turner, R. R. 1982. Atmospheric deposition of metals to forest vegetation. *Science 215*, 1609–1611.

MacMahon, T. A. and Denison, P. J. 1979. Empirical atmospheric deposition parameters—A survey. *Atmos. Environ. 13*, 571–585.

Malone, R. C., Pitcher, E. J., Blackmon, M. L., Puri, K. and Bourke, W. 1984. The simulation of stationary and transient geopotential height eddies in January and July with a spectral general circulation model. *J. Atmos. Sci. 8*, 1394–1419.

Matthews, E. 1983. Global vegetation and land use: New high resolution data bases for climate studies. *J. Clim. Meteorol. 22*, 474–487.

Matthews, E. 1984. Prescription of land-surface boundary conditions in GISS GCMII and vegetation, land-use and seasonal albedo data sets: documentation of archived data tape, NASA Technical Memos 86096 and 86107, NASA, Goddard Institute for Space Science, New York.

Moller, U. and Schumann, G. 1970. Mechanisms of transport from the atmosphere to the earth's surface. *J. Geophys. Res. 75*, 3013–3019.

Pitcher, E. J., Malone, R. C., Ramanathan, V., Blackmon, M. L., Puri, K. and Bourke, W. 1983. January and July simulations with a spectral general circulation model. *J. Atmos. Sci. 40*, 580–604.

Pruppacher, H. R. and Klett, J. D. 1978. Microphysics of Clouds and Precipitation, D. Reidel, Hingham, Mass., 714 pp.

Ramanathan, V., Pitcher, E. J., Malone, R. C. and Blackmon, M. L. 1983. The response of a spectral general circulation model to refinements in radiative processes. *J. Atmos. Sci. 40*, 605–630.

Russell, I. J., Choquette, C. E., Fang, S. L., Dundulis, W. P., Pao, A. A. and Pszenny, A. A. P. 1981. Forest vegetation as a sink for atmospheric particulates: Quantitative studies in rain and dry deposition. *J. Geophys. Res. 86*, 5347–5363.

Sehmel, G. A. and Sutter, S. L. 1974. Particle deposition rates on a water surface as a function of particle diameter and air velocity. *J. Rech. Atmos. 8*, 911–920.

Slinn, S. A. and Slinn, W. G. N. 1980. Predictions for particle deposition on natural waters. *Atmos. Environ. 14*, 1013–1016.

Slinn, W. G. N. 1977. Dry deposition and resuspension of aerosol particles—a new look at some old problems. In: Atmosphere-surface exchange of particulate and gaseous pollutants. ERDA Symposium Series, Richland, WA, 4–6 Sept. 1974, 1–60, CONF-740921, NTIS.

Slinn, W. G. N. 1982. Prediction for particle deposition to vegetative canopies. *Atmos. Environ. 16*, 1785–1794.

Slinn, W. G. N. 1983. A potpourri of deposition and resuspension questions. In: *Precipitation Scavenging, Dry Deposition, and Resuspension* (eds. H. R. Pruppacher, R. G. Semonin, and W. G. N. Slinn). Elsevier, New York, 1361–1416.

Slinn, W. G. N., Hasse, L., Hicks, B. B., Hogan, A. W., Lal, D., Liss, P. S., Münnich, K. O., Sehmel, G. A. and Vittori, O. 1978. Some aspects of the transfer of atmospheric trace constituents past the air-sea interface. *Atmos. Environ. 12*, 2055–2087.

Walcek, C. J., Brost, R. A., Chang, J. S. and Wesely, M. L. 1986. SO_2, sulfate and HNO_3 deposition velocities computed using regional landuse and meteorological data. *Atmos. Environ. 20*, 949–960.

Wesely, M. L., Cook, D. R., Hart, R. L. and Speer, R. E. 1985. Measurements and parameterization of particulate sulfur dry deposition over grass. *J. Geophys. Res. 90*, 2131–2143.

Whitby, K. T. 1978. The physical characteristics of sulfur aerosols. *Atmos. Environ. 12*, 135–159.

Whitby, K. T. and Cantrell, B. K. 1975. Atmospheric aerosols, characteristics and measurements, Presented at the *Int. Conf. on Environmental Sensing and Assessment*, Las Vegas, NV.

Williams, R. M. 1982. A model for the dry deposition of particles to natural water surfaces. *Atmos. Environ. 16*, 1933–1938.

Williamson, D. L. 1983. Description of NCAR community climate model (CCM0B). NCAR Technical Report, NCAR/TN-210 + STR.

Williamson, D. L. and Williamson, G. S. 1984. Circulation statistics from January and July simulations with the NCAR community climate model. NCAR Technical Note, NCAR/TN-244 + STR.

Wilson, M. F. 1984. The construction and use of land surface information in a general circulation climate model. Unpublished Ph.D. thesis, University of Liverpool, U.K.

Wilson, M. F. and Henderson-Sellers, A. 1985. A global archive of land cover and soils data for use in general circulation climate models. *J. Climatol. 5*, 119–143.